15.   The Dynamic Radical Pair at High Field

We now consider the dynamic radical pair in a high magnetic field. These are the typical conditions under which magnetic resonance measurements are made and under which ISC of the pair may be strongly influenced by the coupling of electron and nuclear spins to the applied field. First let us consider the effect on the applied field on the triplet and singlet energy surface (Figure 33). At zero field there is a single triplet energy surface because the three triplet sublevels (T_-, T_+ and T_0) are degenerate. At high field the three surfaces are split in energy, with T_0 maintaining the same magnetic energy it had at zero field, with T_- decreasing in energy as the result of Zeeman coupling and with T_+ increasing in energy as the result of Zeeman coupling.

Figure 33, as Figure 32, can be analyzed in terms of four regions: (1) region 1 for which the singlet triplet splitting is much larger than the Zeeman energy; (2) region 2 for which the singlet triplet splitting is of the order of the Zeeman interaction; (3) region 3 for which the singlet triplet splitting is zero, but the dynamic pair is geminate and is likely to experience reencounters; and (4) region 4 for which the singlet splitting is zero but the dynamic pair is separated to such large distance that the probability of a reencounter is vanishlying small and the pair can be viewed as a random pair or free radicals. We note in particular from the standpoint of ISC, that ISC of the geminate dynamic pair is not likely in region 1 (large S-T gap quenches ISC), that in region 2 a $T_- \varnothing$ S surface "crossing" occurs and provides a pathway for ISC and that in region 3 a $T_0 \varnothing$ S surface "touching" occurs and provides a pathway for ISC.

ESR spectrum of weakly correlated dynamic spin pairs. Spin Correlated Radical Pairs in Regions 2 and 3.

As discussed above, a dynamic geminate radical pair experiences a fluctuation between large values of J (contact pair, region 2, Figures 32 and 33) and weak value of J (solvent separated pair, region 3, Figure 32 and 33). Irreversible separation of the pair into random radicals competes with the oscillation of the pair back and forth between the contact and solvent separated states, i.e., reencounters. Let us now consider the ESR spectra expected for the pair in each of the regions. In region 2 if the magnitude of J is sufficiently large, the ESR spectrum is expected to be similar to that of the molecular triplet discussed in section 12. However, in fluid solution, because of the effects of dipolar interactions between the coupled spins and molecular rotation, the ESR spectrum is not a series of relatively sharp lines corresponding to transitions between well defined magnetic energy levels, but a is a broad, difficultly measurable spectrum corresponding to a wide range of transition for each possible molecular orientation in the magnetic field.
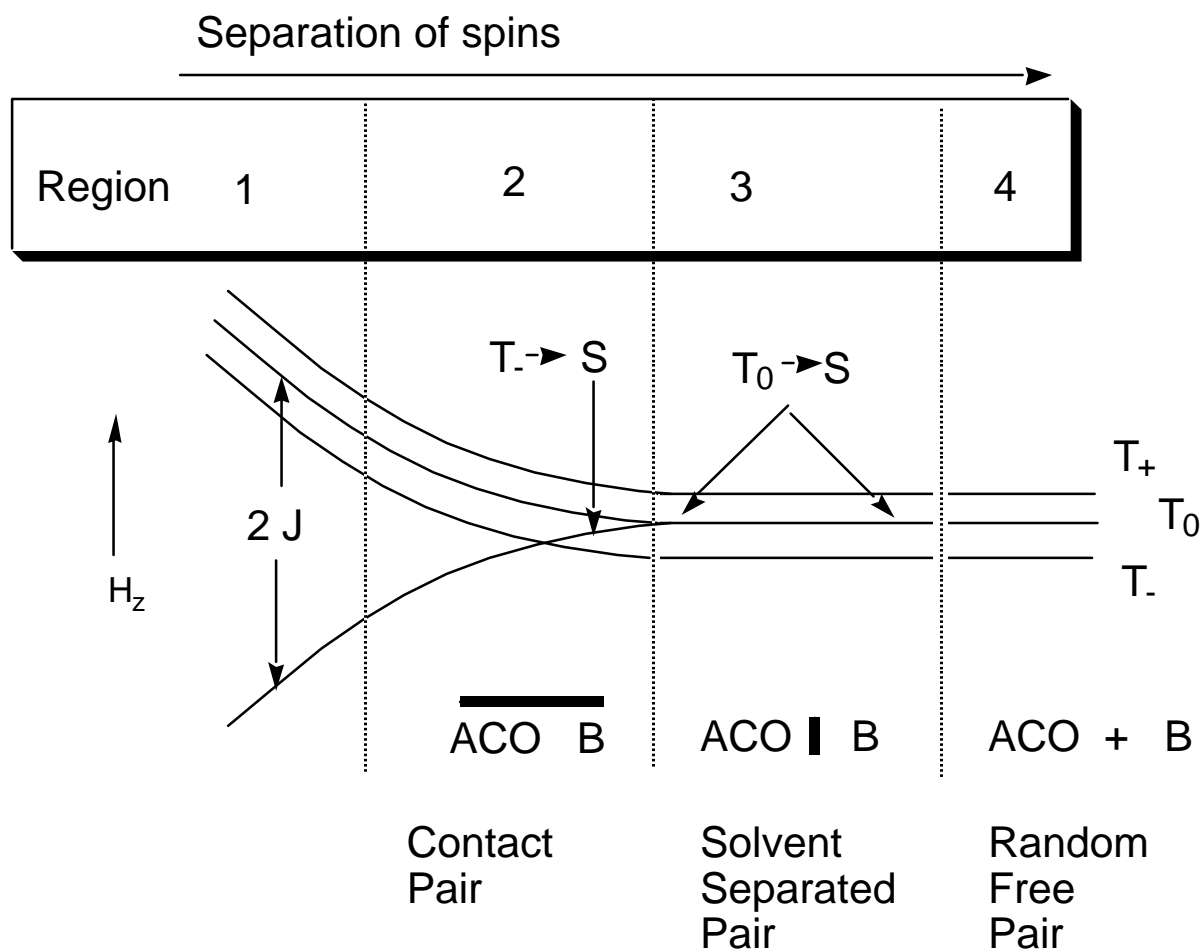
Figure 33. Effect of Zeeman splitting on the energy surface for the α-cleavage of a triplet ketone.

However, in region 3 the magnitude of J is small relative to the Zeeman coupling so that the spins are weakly correlated to each other, but strongly coupled to the applied field. It is therefore possible to consider a pair in this region as **spin correlated radical pair** (SCRP) whose ESR is determined by the doublet character of the individual radicals. Furthermore, during the excursions between the contact and separated states the radical partners of the pair undergo many rotations so that the dipolar magnetic interactions are small (Eq. 28) and may be averaged to zero. As a result, the ESR of a dynamic radical pair is expected consider of relative sharp signals and to be observable if an ESR measurement can be made during the lifetime of the dynamic radical pair. Experiments are possible through time resolved ESR instruments which are capable of time resolutions of ca 100 ns. However, dynamic geminate radical pairs in homogeneous solutions generallly possess lifetimes much shorted than 100ns, the lifetime of the geminate pair must be extended by some sort of constraint which delays separation into random radicals. This can be done either

molecularly by attaching the spins through a flexible covalent linkage or supramolecularly by adsorbing the spins non-covalently in a constrained space such as a micelle.

As a model for the ESR of SCRP, we consider the magnetic energy diagram shown in Figure 34 for our prototype geminate pair, $ACO\cdot\ \cdot B$. In the absence of any exchange interaction T_0 and S have precisely the same energy and the Zeeman splitting of T_- and T_+ from T_0 are identical. Thus, the ESR consists of a single line due to two overlapping transitions at ω_0 ($T_- \varnothing T_0$ and $T_0 \varnothing T_+$, Figure 34, left). In the presence of an exchange interaction that is weak relative to the Zeeman interactions, and in the presence of some coupling of the S and T_0 states (through hyperfine coupling, spin orbit coupling, etc.) the S and T_0 states split and create the new energy level diagram shown in Figure 34 (middle).

The number of transitions observed experimentally will depend on the extent of state mixing and electron exchange, which will determining the probability of transitions between the various levels. For example, if the mixing is strong, transitions between the nominal S and T levels can be observed. On the right of Figure 34 is shown one of the simplest cases: the net effect is raising the energy of the T_0 state so that the $T_- \varnothing T_0$ transition occurs at higher frequency than the $T_0 \varnothing T_+$ transition. When such is the case, the frequency difference between the transitions can be related to the magnitude of the electron exchange, J. Inspection of the energy diagram shows that the splitting between two adjacent transitions is equal to J, the singlet triplet splitting. The situation is exactly analogous to that for NMR splitting for which the separation between adjacent transition is equal to the nuclear spin-spin splitting.

T+ ω_0 T$_0$ ω_0 T$_-$ — S

$J = 0, H_i = 0$

T+ ω_2 T$_0$ 2J ω_1 S T$_-$

$J \circ 0, H_i = 0$

T+ ω_2 T$_0$ 2J ω_1 S T$_-$

$J \circ 0, H_i \circ 0$

H$_{ext}$

ω_o

ω_1 ω_2 ω_o 2J

ω_1 ω_2 ω_o 2J

| Boltzmann No S-T splitting | Boltzmann Small S-T splitting | Polarized due to reaction of S |
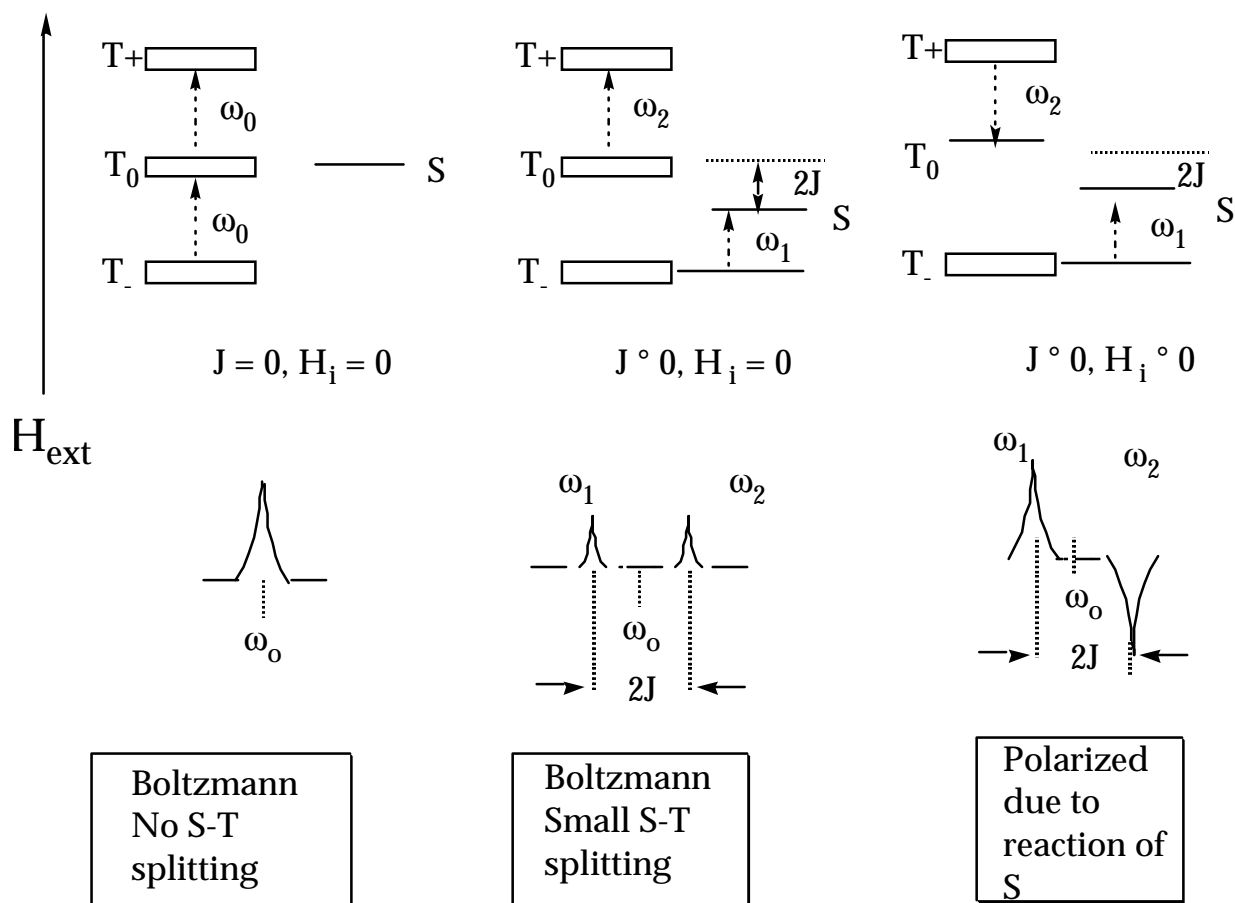
Figure 34. Schematic representation of the effect of exchange interaction and S-T mixing on the ESR spectrum of a weakly spin correlated radical pair.

The ESR of a spin correlated dynamic radical pair in homogeneous solution has not been observed by conventional ESR spectroscopy, but has been observed through time resolved polarized ESR spectroscopy. The basic idea behind the polarization is that because of the mixing of the S and T$_0$ levels, the T$_0$ level is selectively depleted through ISC and as a result the T$_-$ and T$_+$ states are "overpopulated". Since the probability of radiative transitions is related to population differences (Eq. 27, Figure 25) the probability of transitions to T$_0$ from the T$_-$ and T$_+$ states occur well above the probability of transitions due to the Boltzmann population. The experimental result is that instead of two absorptive signals corresponding to the weaker Boltzmann population (Figure 34, middle), there will be one absorptive signal at low frequency (ω_1) and an enhanced emission signal at high frequency (ω_2). This is a striking prediction and is observed experimentally for many biradicals and supramolecular radical pairs in micelles. For these systems the conditions for a long lived geminate pair are optimal.

ESR of Radicals Produced from Spin Selective Intersytem Crossing.

We have seen that the intersystem crossing step, $S_1 \varnothing T$ leads to the specific population of one of the three triplet levels and that for a ketone this is typically the highest magnetic sublevel (T_z). The selectivity results from spin orbit coupling, which favors the coupling of the spin to the z axis of the molecular frame. Immediately after ISC, the T_z level is overpopulated and the lower energy T_x and T_y levels are underpopulated relative to the equilibrium populations dictated by the Boltzmann distribution (Figure 29). The spin system will begin to rapidly equilibrate the three triplet sublevels through spin lattice relaxation. However, if the triplet unders a reaction to produce a radical pair ($^{*3}R\varnothing{}^3RP$), the overpopulation of the T_z may be carried over to the radicals of the geminate pair and then to the free radicals after pair separation. The time scale of spin lattice relaxation among the triplet sublevels is of the order of 10^9 s^{-1}. Thus, the rate of α-cleavage must be of this order to compete with spin lattice relaxation and carry the polarization over to the radicals, $ACO\cdot\ \cdot B$ (for simplicity we ignore hyperfine coupling). If this occurs the resulting free radicals are overpopulated in the D_+ levels. .

Figure 35 schematically shows the process $S_1 \varnothing T_z \varnothing T_+ \varnothing ACO\cdot (D_+) + B\cdot (D_+)$. The time of spin relaxation of free radicals is of the order of microseconds, which is well within the time scale of conventional time resolved ESR spectroscopy, so that polarized radicals can be readily detected experimentallyTypically, the $ACO\cdot$ radical has a smaller g factor ($g_1 \sim 2.001$) than $B\cdot$ ($g_2 \sim 2.003$) radicals that are carbon centered. The observed spectrum of the radicals consists of two signals, one for each radicals and is identical in frequency to that for the radicals at the Boltzmann; however, the **entire** spectrum is in **emission** rather than absorbtion. Experimentally, the observatino of such an emission is evidence that the $S_1 \varnothing T_z \varnothing T_+$ steps have occured and that $S_1 \varnothing T$ ISC is spin sublevel selective. Thus, this example shows how the time resolved ESR of free radicals, produced by the reaction of triplets, can provide indirect information on the S_1 to T ISC crossing step preceeding the formation of a triplete radical pair! It is an excellent example of "spin memory" and the fact that even in solution at room temperature spin

Figure 35. Schematic of the pathway of electron spins from sublevel ISC to cleavage to form spin polarized random radicals.

relaxation may be sufficiently slow as to be measured by both direct (polarized radicals) and indirect means (inferred mechanism of polarization).

ESR of Radicals Containing a Hyperfine Coupling

Radical pairs in regions 2 and 3 possess correlated electron spins. We have seen how the correlation or coupling of two electron spins can influence observed ESR spectra and how ESR spectra of correlated electron spins can lead to information on the electronic structure of triplet states and the mechanism of ISC. Now we consider the coupling of a single electron spin with a magnetic nucleus influences the ESR spectrum of a radical and the ISC of a radical pair. In actual cases it is usually the rule that an electron spin will be coupled to more

than one nuclear spin. However, the basic featurtes of the ESR of an electron spin coupled to a single nulcleus of spin 1/2 will reveal most of the basic features of the ESR of carbon radicals, the most important family of radicals invovled in organic photochemical reactions.

ESR of Radical Pairs in Regions 3 and 4.

The energy diagram for an electron coupled to a nuclear spin of 1/2 is shown in Figure 15. Figure 36 compares the energy level diagram for the spinomeric radicals $A^{12}CO\cdot$ and $A^{13}CO\cdot$. We recall from Eq. 14 that the frequencies, ω, at which the ESR signals of radicals without hyperfine couplings are observed is related to the energy differences between the energy levels. These energy differences are readily computed for our simple example of a single hyperfine coupling from Eq. 31. We note that the magnetic energy of the hyperfine levels depend on two quantum numbers: M_S the quantum number for the electron spin and M_I the quantum number for the coupled nucleus. In addition the energy depends on the hyperfine coupling constant, a and the Zeeman terms, g_1 , μ_e, and H_Z.

$$E_{SI} \ = \ \backslash\omega = \ M_S g_1 \mu_e H_Z + M_I M_S a \qquad (31)$$

The energies of the magnetic levels, computed from Eq. 31, are listed in Figure 36. The frequencies for the ESR transitions are obtained by dividing the right hand of Eq. 31 by $\backslash$ (Eq. 32).

$$\omega \ = \ [M_S g_1 \mu_e H_Z + M_I M_S a]/\backslash \qquad (32)$$

The frequencies of the ESR signals for the $A^{12}CO\cdot$ and $B\cdot$ radicals (a assumed to be zero) occur at frequencies $g_1\mu_e H_Z/\backslash$ and $g_2\mu_e H_Z/\backslash$, where g_1 and g_2 are the g factors of the $A^{12}CO\cdot$ and $B\cdot$ radicals, respectively.

From Eq. 32 we note that in the absence of hyperfine coupling (a = 0), the frequency at which the signal is observed depends only on the g factor and the magnetic field strength. In the presence of a single hyperfine coupling, the energy levels correspond to those of Figure 36. Recall that the allowed ESR transitions are between the levels for which the electron spin changes orientation ($\beta_\epsilon \ \oslash \ \alpha_e$) but the nuclear spin orientation is conserved. The observed spectrum of the radical $A^{13}CO\cdot$ thus consists of two lines, whose frequencies, $\omega_1{}^\alpha$ and $\omega_1{}^\beta$, are given by Eq. 33 and 34, for $M_s = +1/2$ and $M_s = -1/2$, respectively. We label the frequencies ω_α and ω_β for the quantum numbers $M_s = +1/2$ and $M_s = -1/2$, respectively.

$$\omega_1{}^\alpha = g_1\mu_e H_Z/2\backslash + a/4 \tag{33}$$

$$\omega_1{}^\beta = g_1\mu_e H_Z/2\backslash - a/4 \tag{34}$$

$$A^{12}\overset{\bullet}{C}O\ (g_1 = 2.001)$$

$$\overset{\bullet}{B}\ (g_2 = 2.003)$$

$$E_2{}^+ = +(1/2)g_2\mu_0 H_Z$$
$$\alpha_e$$

$$E_1{}^+ = +(1/2)g_1\mu_0 H_Z$$
$$\alpha_e$$

$$\omega_1 \qquad \Delta E_1{}^0 = g_1\mu_0 H_Z$$

$$\omega_2 \qquad \Delta E_2 = g_2\mu_0 H_Z$$

$$\beta_e$$
$$E_1{}^- = -(1/2)g_1\mu_0 H_Z$$

$$\beta_e$$
$$E_2{}^- = -(1/2)g_2\mu_0 H_Z$$

$$E_1{}^+ + a/4 \qquad\qquad\qquad \alpha_e\alpha_n$$

$$E_1{}^+ - a/4 \qquad\qquad\qquad \alpha_e\beta_n$$

$$\Delta E_1{}^\beta = g_1\mu_0 H_Z - a/2 \qquad\qquad \Delta E_1{}^\alpha = g_1\mu_0 H_Z + a/2$$

$$E_1{}^- + a/4 \qquad\qquad\qquad \beta_e\beta_n$$

$$\omega_1{}^\beta \qquad \omega_1{}^\alpha$$

$$E_1{}^- - a/4 \qquad\qquad\qquad \beta_e\alpha_n$$
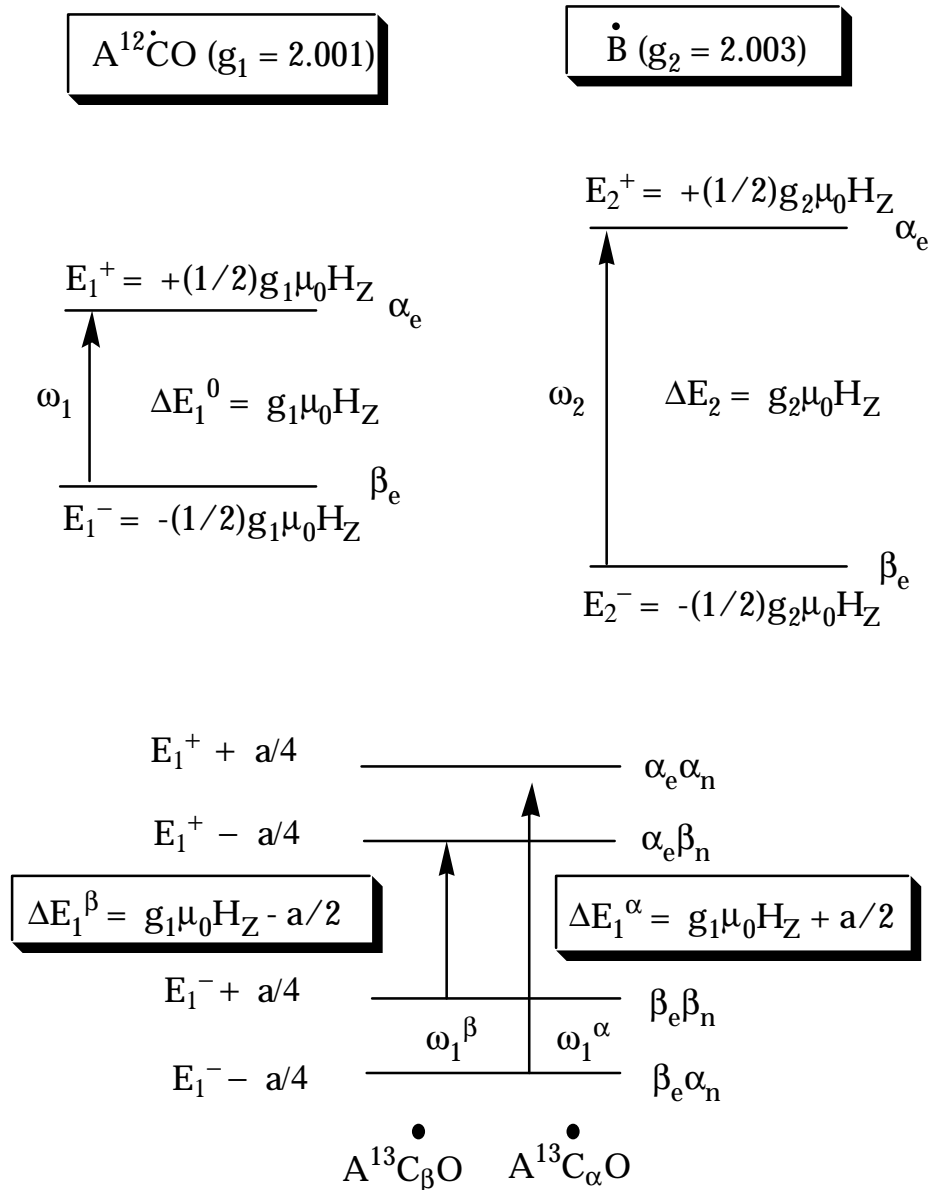
$$A^{13}\overset{\bullet}{C}_\beta O \qquad A^{13}\overset{\bullet}{C}_\alpha O$$

Figure 36. Energy level diagrams for the radicals $A^{12}CO$, $A^{13}CO$ and B. See text for discussion.

The ESR of the $A^{12}CO$ and $A^{13}CO$ radicals

Figure 37 displays the ESR spectra of a solution containing an equal number of $A^{12}CO\cdot$ and $B\cdot$ radicals (top) and a solution containing an equal number of $A^{13}CO\cdot$ and $B\cdot$ radicals (bottom). In the absence of hyperfine coupling the spectrum of the (separated) $A^{12}CO\cdot$ and $B\cdot$ radical pair consists of two signals: one at $\omega_1 = g_1\mu_e H_Z/\backslash$ ($A^{12}CO\cdot$) and one at $\omega_2 = g_2\mu_e H_Z/\backslash$ ($B\cdot$). For a typical g_1 of 2.001 for the $A^{12}CO\cdot$ a radical and a typical g_2 of 2.003 for the $B\cdot$ radical, the ESR signal of the $A^{12}CO\cdot$ radical will occur at lower frequency, since ω is directly proportional to g at a fixed field.

In the presence of the single ^{13}C hyperfine coupling, the spectrum of the (separated $A^{13}CO\cdot$ and $B\cdot$ radicals consists of three signals: one at $\omega_2 = g_2\mu_e H_Z/\backslash$ ($B\cdot$) and two split symmetrically by a/2 Gauss about the frequency $\omega_1 = g_1\mu_e H_Z/\backslash$. The signal at lower frequency is labeled ω_1^{α} and corresponds to the ESR of the spinomer $A^{13}CO(\alpha_n)$, i.e., the carbonyl radical possessing a nuclear spin with α orientation with respect to the magnetic field. The signal at higher field is labeled ω_1^{β} and corresponds to the ESR of the spinomer $A^{13}CO(\beta_n)$, i.e., the carbonyl radical possessing a nuclear spin with β orientation with respect to the magnetic field. Since ω_1 is the frequency for the $A^{12}CO\cdot$ transition, then the frequencies of the ω_α and ω_β transitions are given by Eqs. 35 and 36, respectively. Thus, the ESR spectrum of the free $A^{13}CO\cdot$ and $B\cdot$ radicals consists of three signals consists of three lines: (1) a low frequency line whose frequency is $\omega_1^{\beta} = \omega_0 - (a/2)/\backslash$; (2) a medium frequency line whose frequency is ω_2; and a high field line whose frequency is $\omega_1^{\alpha} = \omega_0 + (a/2)/\backslash$. A typical hyperfine coupling for a $A^{13}CO\cdot$ radical is 120 Gauss.

$$\omega_1^{\alpha} = \omega_1 + (a/2)/\backslash \qquad\qquad (35)$$

$$\omega_1^{\beta} = \omega_1 - (a/2)/\backslash \qquad\qquad (36)$$

In Figure 37, a vector model representation of the magnetic basis of the hyperfine coupling is shown. A nucleus with an α orientation possesses a magnetic moment vectors that points in the direction of the applies field. Thus the electron experiences not only the applied field, H_z, but also the hyperfine field a/2, which augments the applied field. The electron precesses **faster** in the higher field $H_z + a/2$ than it does in H_z alone. On the other hand, a nucleus with an β orientation possesses a magnetic moment vectors that points opposed to the direction of the applied field. Thus the electron experiences not only the applied field, H_z, but also the hyperfine field a/2, which dimunishes the applied

field. The electron precesses **slower** in the higher field $H_z - a/2$ than it does in H_z alone.

$g_1 = 2.001$

ω_1

ω

ω_2 $g_2 = 2.003$

ω

A $\overset{O}{\underset{12}{\overset{\|}{C}}}$ ·

B ·

$g_1 = 2.001$

β α

a $= 60$ G   **a** $= 60$ G

ω

H_0 H_0

$g_2 = 2.003$

A $\overset{O}{\underset{13}{\overset{\|}{C}}}$ ·

α spin precesses faster (sees a stronger field)

β spin precesses slower (sees a weaker field)

ω

$\omega_1{}^{\beta}$ ω_1 ω_2 $\omega_1{}^{\alpha}$ B ·
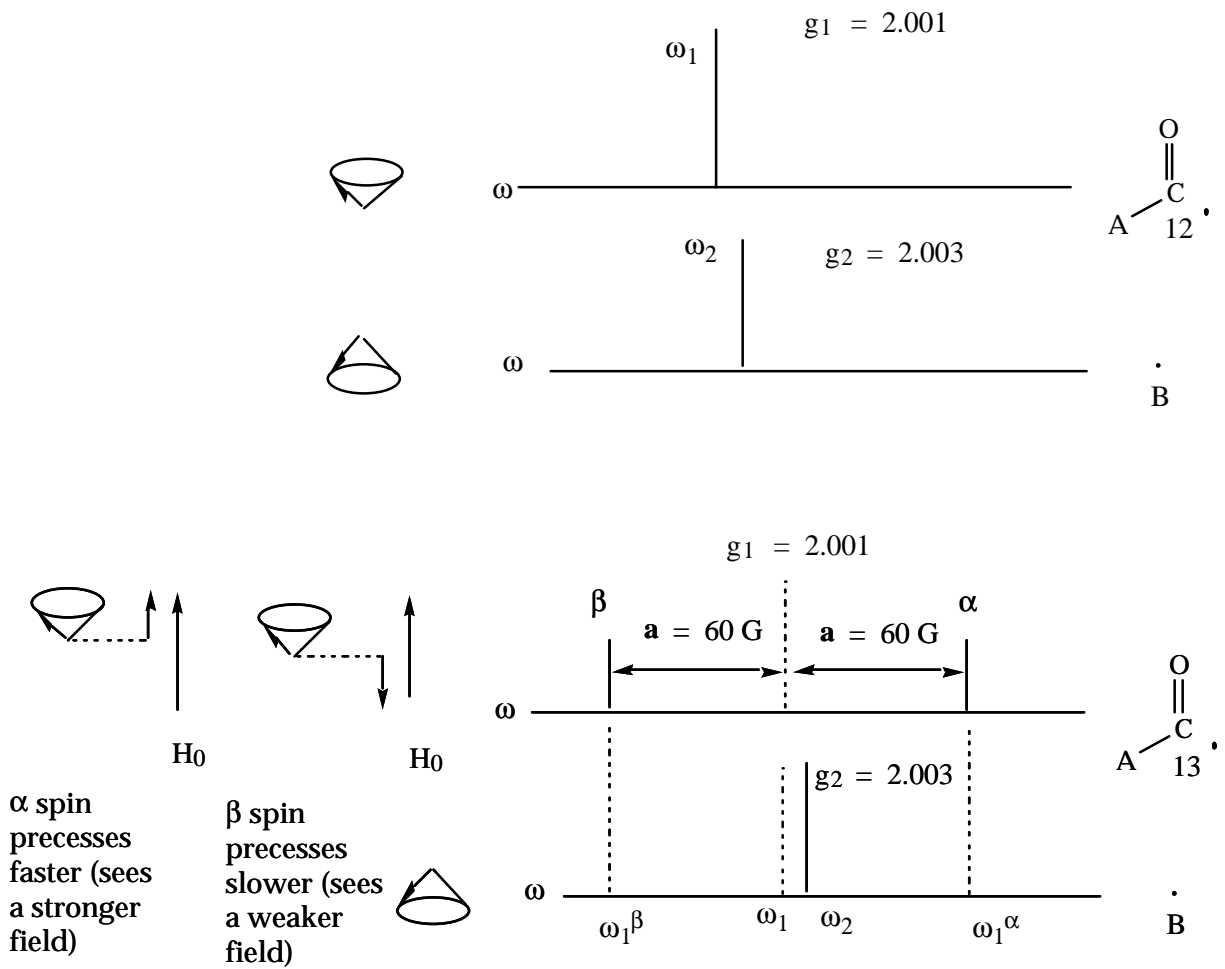
Figure 37. Schematic of the ESR of two spinomeric free radical pairs. Top: the A^{12}CO B pair. Bottom: the A^{13}CO B pair.